Effect of pressure on the atomic volume of Zn, Cd, and Hg up to 75 GPa

Olaf Schulte and Wilfried B. Holzapfel
Universität-GH Paderborn, D-33095 Paderborn, Germany
(Received 6 July 1995)

The elemental metals Zn, Cd, and Hg are studied under pressure in a diamond-anvil cell by energy-dispersive x-ray diffraction. While Zn and Cd remain in the $hP2$ structure up to the highest pressures achieved, several phase transitions are observed in Hg with a $hP2$ structure for the high-pressure δ-Hg phase. Different equation of state (EOS) forms are fitted to these experimental data and, for comparison, also to literature data of Be and Mg. A detailed analysis of the data shows that a simple one parameter EOS form describes the isothermal behavior of almost all the phases. Only the intermediate γ-Hg phase shows slight deviations from this ''simple'' EOS behavior.

I. INTRODUCTION

Progress in pressure generation with diamond-anvil cells and suitable x-ray-diffraction techniques[1] resulted in the unique opportunity to study not only equations of state (EOS's) but also structural parameters of crystalline solids in a pressure range previously accessible only to shock-wave experiments. A comparison of EOS data with different EOS forms allows us to discriminate between more or less suitable forms when accurate low-pressure data are used together with data for these new extended p-V regions, and some specific forms[2,3] allow us to distinguish between ideal, simple, and more complex compressional behavior by comparison with asymptotic laws.[4–10] This type of analysis illustrates with the present data of Zn, Cd, and Hg, together with previous data for Be and Mg, some systematic trends that give some hints for special contributions from inner filled and outer unfilled d-electron shells for some of these elements.

II. EXPERIMENTAL TECHNIQUE

Diffraction patterns of Zn, Cd, and Hg were obtained by energy-dispersive x-ray diffraction (EDXD) using either a conventional x-ray tube with a W anode and the conical slit system in the laboratory[11] or synchrotron radiation at the energy dispersive scattering (EDS) station F3 at HASYLAB, DESY.[12,13] High pressure was generated by a diamond-anvil cell[14,15] with an Inconel X750 gasket, and beveled diamonds with culet diameters of 300 μm were used for pressures above 50 GPa. Pressures were measured with the ruby luminescence technique[16] on the basis of the nonlinear pressure scale.[17] Liquid nitrogen or mineral oil were used as pressure transmitting medium with no notable differences.

III. EDXD RESULTS

A. Zinc

Powder-diffraction patterns of Zn were measured up to 74 GPa. No phase transition was observed in this pressure range, and five lattice spacings d_{hkl} could be used up to the highest pressures for the evaluation of the hexagonal lattice parameters a and c. Since the ratio $c/a=1.8561$ (Ref. 18) deviates at ambient pressure significantly from the value 1.633 of an ideal close packing (of hard spheres), usually referred to as hcp, it seems to be more appropriate to use the strongly recommended Pearson nomenclature[19] $hP2$ for this hexagonal cell with two atoms in its primitive unit. Different slopes in the variations of a and c with pressure, illustrated in Fig. 1, already indicate that c/a must also vary significantly, as shown in Fig. 2. However, in contrast to earlier results from x-ray diffraction at lower pressures,[20] only a monotonous decrease is substantiated by the present measurements. As pointed out previously,[21] deviatoric stresses could be responsible for the unusual variation in c/a in the former experiments. The present results also support a similar observation in a theoretical study.[22] On the other hand, a slight anomaly in c/a near $c/a=\sqrt{3}$ has been observed very recently in an angle-dispersive x-ray-diffraction study[23] because of the higher precision of this method, and this anomaly has been related to an electronic topological transition also noticed in Mössbauer studies at low temperature and high pressure.[24] With increasing pressure above 23 GPa, c/a falls below the ideal hcp value (as shown in Fig. 2) at the compression of $V/V_0=0.74$, whereby V_0 stands for the atomic volume at ambient conditions (V_0(Zn)$=0.015\,22$ nm^3,[18]). The change of volume with pressure is shown in

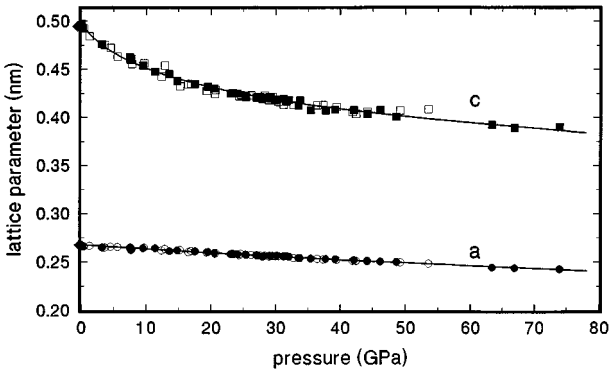

FIG. 1. Lattice parameters of zinc to 74 GPa. Full symbols refer to pressure increasing cycles and open symbols to pressure decreasing cycles, respectively. Diamonds represent the lattice parameters at ambient conditions (Ref. 18). The lines result from a polynomial fit through the data.

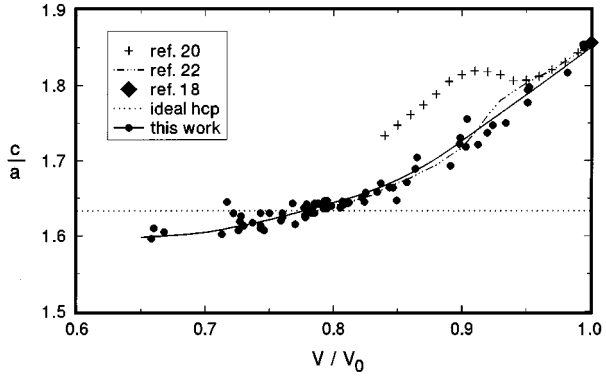

FIG. 2. c/a variation of zinc under pressure. The full line results from the polynomial fit of the single lattice parameters.

Fig. 3 together with data from the literature. In this representation, only minor differences are seen between the results from volumetric high pressure experiments,[25,26] shock wave experiments,[27] and x-ray diffraction.[20]

B. Cadmium

Cadmium shows similar properties like Zn, also at high pressure. The $hP2$ structure remains stable up to the present maximum pressure of 67 GPa, and, as in the case of Zn, the axial ratio decreases from $c/a=1.8855$ (Ref. 18) at ambient conditions to the ideal value of 1.633 at about 50 GPa and finally to $c/a=1.604$ at 68 GPa. For the evaluation of the lattice parameters, only four lattice spacings d_{hkl} could be used over the whole pressure range because of the overlapping of diffraction and fluorescence lines. This effect was partly avoided by additional EDS spectra taken at different diffraction angles. The data for the lattice parameters a and c are shown in Fig. 4, and c/a is plotted in Fig. 5, whereby V_0 stands for the volume at ambient conditions (V_0(Cd)=0.021 58 nm (Refs. 3 and 18). Whereas the earlier x-ray studies[20] resulted in an unusual decrease in c/a, only a monotonous decrease is seen in the present data, and the crossover to values below the value of ideal close packing is similar to the variation in Zn. The variation of the atomic volume for Cd with pressure is shown in Fig. 6 together with data from the literature. Again, only minor differences can be noticed between the volumetric data,[25,26] the shock-wave data,[27] the early x-ray diffraction data,[20] and the present results in this type of representation.

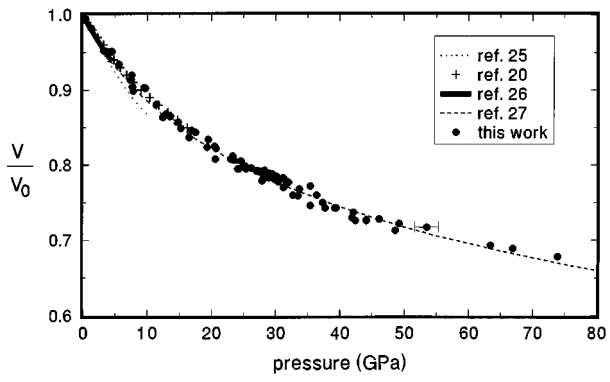

FIG. 3. Pressure-volume data of zinc.

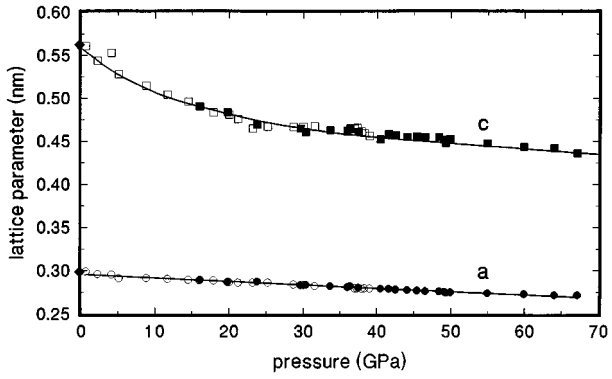

FIG. 4. Lattice parameters of cadmium to 67 GPa. The symbols have the same meaning as in Fig. 1.

C. Mercury

Diffraction patterns of mercury were measured up to 67 GPa. As reported recently,[28] several phase transitions already occur in the lower part of this pressure range (Fig. 7). Besides the well-known rhombohedral ($hR3$, α-Hg) and tetragonal body-centered ($tI2$, β-Hg) phases, an orthorhombic ($oP4$, γ-Hg) and a hexagonal-close-packed ($hP2$, δ-Hg) phase were recently discovered.[28,29]

For clarity, the present representation of the phase diagram for Hg does not include the regions of metastability as discussed in a previous paper, but shows instead best estimates of the triple points and the corresponding equilibrium transition lines. Best values for the slopes of the different boundaries are given in Ref. 28.

The observed lattice spacings, up to 12 d_{hkl} values in the orthorhombic phase, result in the variations of the lattice parameters under pressure as shown in Fig. 8. The variations of the axial ratios are given in Fig. 9. It can be noticed that c/a for δ-Hg starts with a value of 1.7 at the γ-δ phase transition and shows a similar decrease as discussed before for Zn and Cd. A rough estimate indicates that the ideal $hP2$ value for c/a may be reached at a pressure of around 90 GPa corresponding to $V/V_0=0.693$. Also this value is similar to the corresponding crossover values for Zn and Cd. The variation of the atomic volume for mercury under pressure is plotted in Fig. 10. The volume difference for the α-β phase transition at ambient pressure and low temperatures (77 K) is 2%,[18] which compares favorably also with the very small

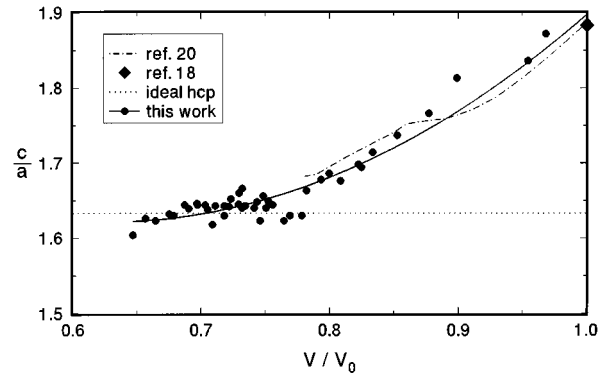

FIG. 5. c/a variation of cadmium under pressure.

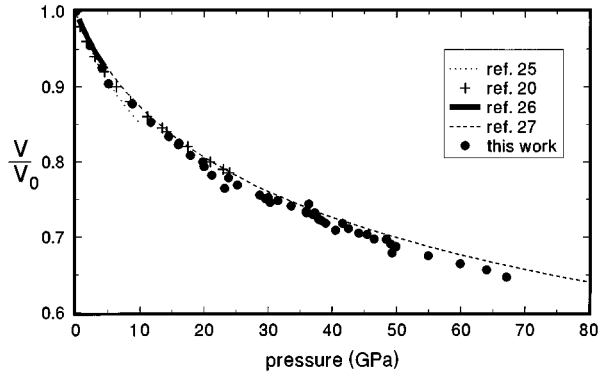

FIG. 6. Pressure-volume data of cadmium.

change observed in the present measurements at room temperature and higher pressures of about 1%.

IV. THE EQUATIONS OF STATE

A. Theoretical background

On the basis of different assumptions, various second- and higher-order forms have been derived over the years to represent EOS data for solids under strong compression, as discussed in detail in Ref. 2. For instance, Murnaghan[30] used the assumption $K(p)=K_0+pK_0'$ with all higher-order pressure derivatives K_0'', K_0''', . . . equal to 0, which results upon integration in the second-order form

$$\text{MU2:}\quad p=\frac{K_0}{K_0'}\left[\left(\frac{V}{V_0}\right)^{-K_0'}-1\right].$$

Birch,[31] on the other hand, expanded the Gibb's free energy F in terms of Eulerian strain

$$\epsilon=X^{-n}-1$$

with $X=(V/V_0)^{1/3}$ and $n=2$, which results in second order in the form

$$\text{BE2:}\quad p=\frac{3}{2}K_0[X^{-7}-X^{-5}]\left\{1-\frac{3}{4}(4-K_0')[X^{-2}-1]\right\}.$$

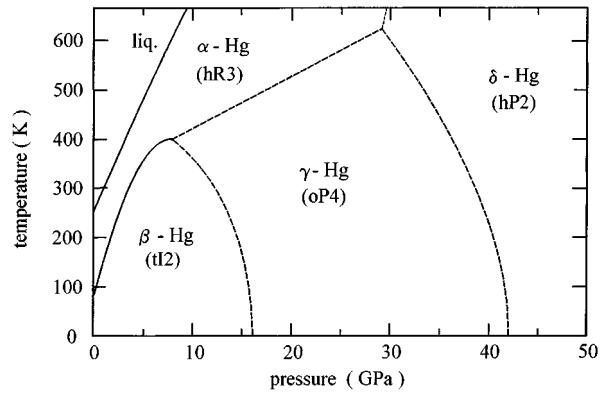

FIG. 7. Pressure-temperature phase diagram of mercury. Details of the diagram are explained in the text.

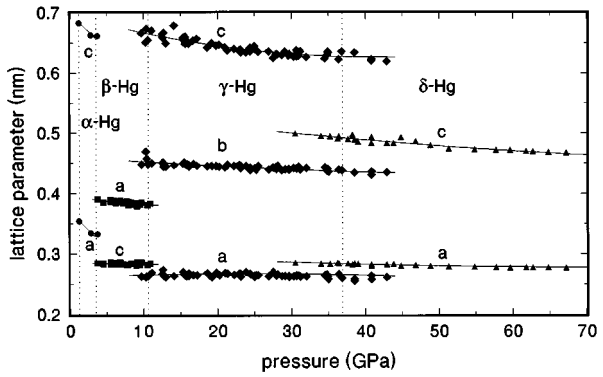

FIG. 8. Lattice parameters of the different high-pressure phases of mercury. The solid lines result from polynomial fits through the data; the dotted lines represent the estimated transition pressures at ambient temperature.

The first-order expansion corresponds in this case to $K_0'=4$, which is a good average value for all kinds of solids.[2]

The use of an effective Rydberg-type potential has been promoted more recently,[32] leading to another second-order form labeled in the later discussion just

$$\text{MV2:}\quad p=3K_0X^{-2}(1-X)\exp\left[\frac{3}{2}(K_0'-3)(1-X)\right].$$

Since all these forms diverge at very strong compression with respect to the well-established Thomas-Fermi limiting behavior,[33,34] more reasonable forms were introduced in recent years[2–4,6,35–37] in the form

$$\text{H02:}\quad p=3K_0X^{-5}(1-X)\exp[c_{02}(1-X)]$$

with $c_{02}=(3/2)(K_0'-3)$, which deviates at ultimate compression only by a constant factor from the Fermi-gas limit

$$p_{\mathrm{FG}}=a_{\mathrm{FG}}(Z/V)^{(5/3)},$$

where Z represents the nuclear charge, V the atomic volume, and $a_{\mathrm{FG}}=23.37$ MPa nm^5 is a universal constant. With the additional condition $c_{02}\rightarrow c_0=-\ln(3K_0/p_{\mathrm{FG0}})$ using $p_{\mathrm{FG0}}=p_{\mathrm{FG}}(V_0)$, H02 retains only K_0 as a free parameter with $K_0'=3+2c_0/3$ fixed by K_0, V_0, and Z. The corresponding first-order form is therefore labeled H11 since it is also related to another second-order form,

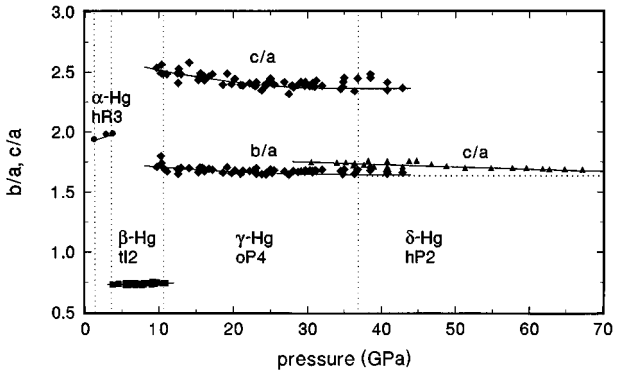

FIG. 9. c/a and b/a variations for the different phases of mercury up to 68 GPa.

H12: $p=3K_0X^{-5}(1-X)\exp[c_0(1-X)+c_{12}X(1-X)]$,

which approaches the correct Fermi-gas limit at ultimate compression and retains one more free parameter $c_{12}=(3/2)(K_0'-3)-c_0$ to represent EOS data as well, which deviate significantly from the simpler H11 form.

In fact, it has been noticed[5,9,10,37] that $c_{12}=0$ is a very good approximation for many ''simple'' solids. The additional condition[3] $c_0=\beta\sigma_0$ with $\beta=5.67$ nm^{-1} and $\sigma_0=(3ZV_0/4\pi)^{1/3}$ is related to the universal Thomas-Fermi scaling at ultimate compression and represents very reasonably the average or ''ideal'' behavior of all kinds of solids even at moderate pressures. Therefore, it is considered as a good zeroth-order approximation with the label H10.

Due to the strong correlations between the parameters K_0 and K_0' in least-squares-fitting procedures generally used to represent the experimental p-V data by one of these second-order forms, more accurate values for K_0 are commonly deduced from ultrasonic measurements taking into account the small correction $K_S/K_T=1+\alpha\gamma T$ between adiabatic (S) and isothermal (T) values, where α, γ, and T stand for the cubic thermal expansion coefficient, the thermodynamic Grüneisen parameter, and the temperature, respectively. For noncubic aggregated (polycrystalline) materials special deviatoric stresses are produced under pressure at the grain boundaries, and only upper[38] and lower[39] limits, known as Voigt and Reuss limits, respectively, can be derived from ultrasonic single-crystal data in these cases for K_0 of the aggregated material.

Thus, a comparison of ultrasonic values with the values for K_0 and K_0' obtained by least-squares fits of any second-order EOS form to experimental p-V data gives usually more rigorous constraints in the attempt to determine the true thermodynamic values of these parameters. In the comparison of ultrasonic values for K_0 with experimental p-V data from various sources covering very different p-V regions, it is very convenient to ''linearize'' the p-V data in such a way that high accuracies at low pressures and strong variations at high pressures are represented on an equal footing.

For the interpolation of experimental EOS data towards the Fermi-gas limit at ultimate compression, a special linearization scheme had been introduced,[3] which uses the scaled pressure coefficient

$$\eta=\ln\frac{p}{p_{\mathrm{FG}}}-\ln(1-X)$$

in $\eta-X$ representations of the experimental data with $X=(V/V_0)^{1/3}$. In this representation of the experimental data, the approach to the asymptotic Fermi-gas behavior at ultimate compression ($X\to 0$) implies $p\to p_{\mathrm{FG}}$ and $\eta\to 0$, and the use of the previously introduced Thomas-Fermi length scale σ_0 results with $\sigma=X\sigma_0$ in one common straight line for all the ideal solids in $\eta-\sigma$ plots. Straight lines with slightly different slopes represent thereby the simple solids.[3] Therefore, $\eta-X$ and $\eta-\sigma$ plots will be used in the following discussion of the present experimental data to gain some deeper insight into the significance of specific EOS forms.

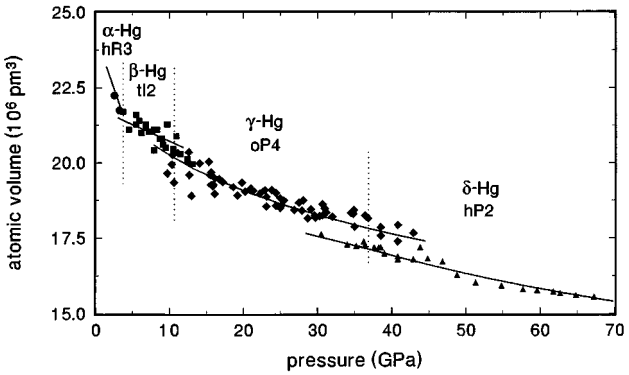

FIG. 10. Pressure-volume data of mercury.

B. Equation of state of Zn

An $\eta-X$ representation of all the previous EOS data for Zn,[20,25–27] together with the present results, is shown in Fig. 11 to illustrate some obvious facts.

(I) The ultrasonic value for K_{T0} (Ref. 40) together with its upper and lower bounds according to the Voigt and Reuss limit[41,42] shows much smaller uncertainties than the experimental EOS data extrapolated to $X=1$.

(II) Bridgman's data[25] deviate systematically at higher compression from all the other data.

(III) The reduced shock-wave data[27] agree perfectly with the present data at the upper end of the present experimental range, however, near ambient pressure, significant deviations from the ultrasonic results can be noticed. The smooth variation of these data comes from the mathematical procedures used in the evaluation of the original shock-wave data and does not represent the true uncertainty of these results.

(IV) The first-order EOS form H11 with the best ultrasonic value for K_0 is represented in this plot by the solid line, which appears to give the best average representation of all the data, including the present results.

Least-squares fits of the different EOS forms to the individual data sets lead to the values for the parameters K_0 and K_0' shown in Table I with standard deviations, which correspond to the condition that the other parameter is fixed at its

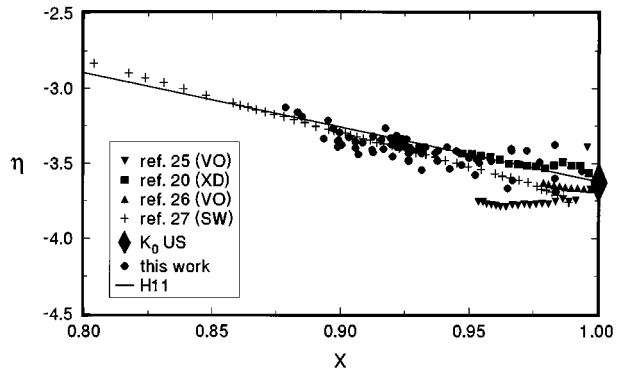

FIG. 11. Comparison of the EOS data of zinc in a $\eta-X$ representation. The vertical size of the diamond represents the scatter of K_0 values from different ultrasonic measurements (Refs. 40–42). VO=volumetric data, XD=x-ray-diffraction data, SW=shock-wave data, and US=ultrasonic data.

TABLE I. Parameters for different EOS forms and different EOS data sets of zinc together with values derived from ultrasonic measurements (US).

K_0 (GPa)	K_0'	p_m (GPa)	σ_V (%)	$-\epsilon$	EOS	Ref.
57(4)	3(1)	10	0.05	0.98		25
68(3)	4.8(7)	25	0.03	0.98		20
60(2)	5(1)	5	0.01	0.97	H12	26
56(1)	6.3(1)	250	0.02	0.99		27
63(2)	5.2(7)	74	0.68	0.52		This work
63(7)	4.6(5)		0.79	0.95	MU2	
57(6)	5.9(9)		0.69	0.89	BE2	
56(6)	6.3(8)	250	0.67	0.89	MV2	All data
56(7)	6.1(8)		0.68	0.99	H02	
56(2)	6.2(8)		0.68	0.53	H12	
61(8)	5.5(1)		0.73		H11	
71						41, *V*
59					US	42, *R*
68.3						40

best value. Strong anticorrelation of these parameters are indicated by the values for the correlation parameter $\epsilon \approx -1$. This anticorrelation is usually much reduced for data covering larger ranges in pressure (p_m) as seen for the present data; however, for the smooth shock-wave results, a large anticorrelation together with small standard deviations is typical, and, in this case, the standard deviations are much smaller than any reasonable uncertainty of the individual parameters as discussed with the more reasonable error ellipsoids presented in Fig. 12. The standard deviations of the volume data with respect to the fitted curve are represented by σ_V. Naturally, very small values for σ_V are noticed for the smooth American Institute of Physics data,[27] whereas σ_V for the present results represents the true experimental precision.

In the first block of Table I only the form H12 was used together with the different sets of data, whereas the second block of Table II shows a comparison of fits with different EOS forms using all the available data. Thereby, MU2 shows the largest value for σ_V, the largest anticorrelation, and a rather poor agreement in the parameter values for K_0 and K_0' in comparison with all the other two parameter fits. BE2, typically, gives slightly larger values for K_0 and smaller values for K_0' than MV2, and both H02 and H12 give values that fall just in between. This observation is typical for EOS data with $K_0' > 4$ and has been noted previously.[6]

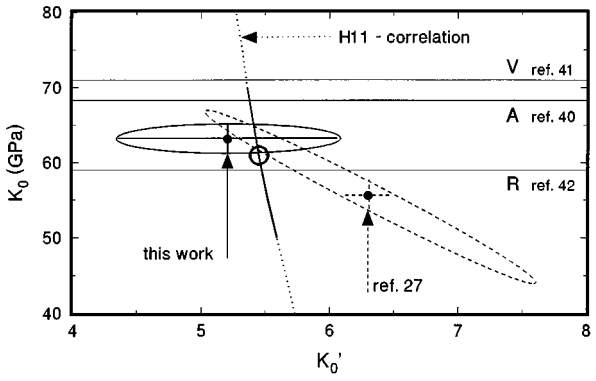

FIG. 12. Error ellipsoids for the parameters obtained by fitting the EOS form H12 to different p-V data sets of zinc. For details see text.

The one parameter fit with the form H11 results in the present case in a slight increase of σ_V and in numerical values for K_0 and K_0' closer to the values of MU2 but still in a perfect agreement with the other sets if one considers just the statistical uncertainties. This situation is also illustrated in Fig. 12, which shows the ultrasonic values for K_0,[40–42] together with the results of fits for the AIP data[27] and for the present data using the form H12. The error ellipsoids, which represent more realistic (correlated) error estimates than the standard deviations, show a common region of overlap for both data sets, and it is interesting to note that the correlation between K_0 and K_0' given by the form $K_0' = 3 - (2/3)\ln(3K_0/p_{FG0})$ implied by H11 intersects this common region close to the value indicated by the circle, which represents the best fitting result of H11 with respect to the present data.

The comparison with the ultrasonic values, given by horizontal lines in Fig. 12, indicates that the average value *A* (Ref. 40) appears to be rather large compared with the present and previous EOS data; however, if one takes into account that polycrystalline bulk materials may show in their EOS behavior any value between the Voigt (V) and Reuss (R) limits, depending on the amount of deviatoric stresses at the grain boundaries, it is only somewhat surprising that the EOS data for strong compression do not approach the hydrostatic Voigt limit of stress continuity (V) but seem to fall closer to the Reuss limit, which corresponds to the strain continuity at the grain boundaries.

The differences between the individual EOS forms are most clearly illustrated in an extended $\eta - X$ plot, as shown in Fig. 13, where the best-fitting parameters from Table I (all data) were used for the individual extrapolations. Obviously, MU2 diverges most rapidly to very large values of η, and BE2 diverges more slowly in the same direction, whereas MV2 diverges in the opposite direction. The differences between H11 and H12 are marginal, and all the differences

TABLE II. Parameters for different EOS forms and different EOS data sets of cadmium together with values derived from ultrasonic measurements (US).

K_0 (GPa)	K_0'	p_m (GPa)	σ_V (%)	$-\epsilon$	EOS	Ref.
39(2)	5.7(9)	10	0.06	0.98		25
46(3)	7.2(7)	24	0.21	0.96		20
45(3)	7.3(8)	24	0.19	0.95	H12	20[a]
45(2)	8.0(9)	5	0.03	0.96		26
49(2)	6.0(2)	120	0.08	0.94		27
46(4)	6.0(7)	68	0.86	0.98		This work
48(6)	5.0(5)		0.99	0.98	MU2	
44(5)	6.0(9)		0.86	0.89	BE2	
43(5)	6.6(9)	120	0.84	0.94	MV2	All data
44(6)	6.4(9)		0.85	0.95	H02	
43(5)	7.0(9)		0.84	0.93	H12	
48(8)	5.7(1)		0.87		H11	
54.4						43, *V*
44.4						43, *R*
62.2					US	45, *V*
44.5						45, *R*
52.9						44

[a]Rescaled data, as discussed in the text.

between H02, H12, and H11 just give a measure for the uncertainties in the intermediate region. Finally, it can be noticed also for later discussion that Zn is softer than the ideal solid behavior, which is represented by the dotted straight line in Fig. 13.

C. Equation of state of Cd

The $\eta-X$ plot of the different literature data for Cd,[20,25–27] together with the present data in Fig. 14 shows slightly lower values for the present results in comparison with the shock-wave data.[27] Bridgman's data[25] are significantly lower, but with the correct slope, and the data from Lynch and Drickamer[20] display an unusual change in slope together with an apparent divergence at $X=1$. This variation is typical for V/V_0 data, which were reduced by an inconsistantly small value for V_0 in comparison with other data. If, therefore, one rescales these data with a $V_R=0.021\,45$ nm^3 instead of the true V_0, one obtains the results shown in Fig. 14 as solid squares, which agree more reasonably with all the other more recent data.

Table II first presents the results of fitting the form H12 to the individual data sets. The differences in the values for K_0 and K_0' remain within the statistical errors for all the data sets except for the data of Bridgman.[25]

The error ellipsoids of these fits are illustrated in Fig. 15 for the different data sets from the literature[20,26,27] and for the present data. It can be noticed that the data for smaller pressure ranges result in larger values of K_0'. The error ellipsoids of the different data sets overlap significantly only in the region that is also intersected by the correlation of the H11 form.

The middle part of Table II compiles the results of fits with different EOS forms using all the p-V data of cadmium.

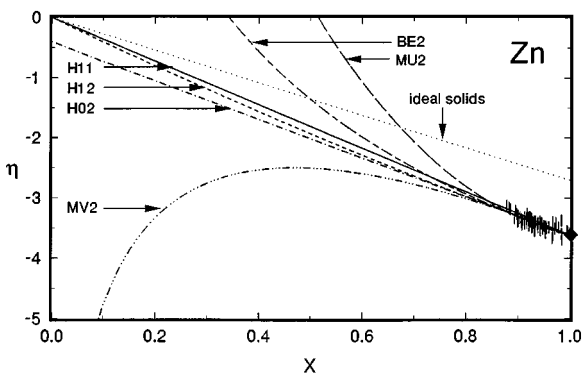

FIG. 13. $\eta-X$ representation of different EOS forms for zinc. The diamond gives the best value of K_0 derived from ultrasonic measurements (Ref. 40). The bars indicate only the present data.

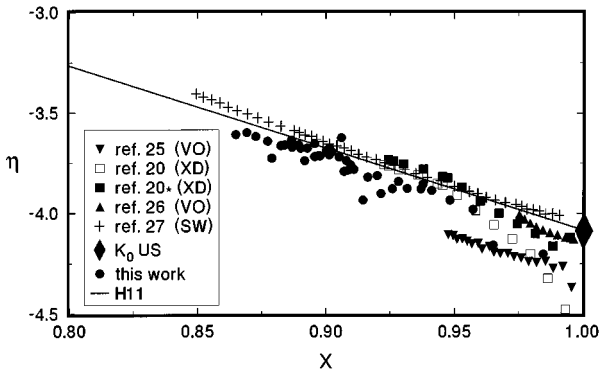

FIG. 14. Comparison of the EOS data of cadmium in a $\eta-X$ representation. The vertical size of the diamond represents the scatter of the K_0 values from different ultrasonic measurements (Refs. 43–45). The star denotes rescaled data as discussed in the text and footnote of Table II.

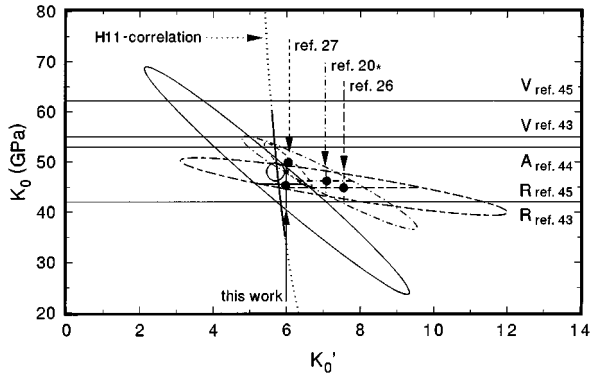

FIG. 15. Error ellipsoids for the parameters obtained by fitting the EOS form H12 to different p-V data sets of cadmium. For details see the text. The star on Ref. 20 denotes rescaled data as discussed in the text and footnote of Table II.

Obviously, the forms BE2, MV2, H02, and H12 give almost the same results; however, the form MU2 leads to a significant difference for the value of K_0' and also to a larger value of σ_V. A fit of the one parameter form H11 to the data shows no significant deviation, as illustrated also in Fig. 15 by the circle, which fits very close to the region of overlap for the different EOS data right in the middle between the most recent values for K_0 derived from ultrasonic (US) data.[43,44]

The differences in the individual best-fit EOS curves are shown in the $\eta-X$ plots of Fig. 16. Again, the divergence of the forms MU2, BE2, and MV2 at very strong compression is obvious. In comparison with the curve of an ideal solid, a softer behavior of Cd can be noticed, represented by its lower values of η.

In summary, the high-pressure behavior of both zinc and cadmium is well described with the one parameter form H11. The use of two parameter forms H12 or H02 does not lead to a significant improvement of the fit. The more commonly used forms MU2, BE2, and MV2 show no advantage but only their common divergences at strong compression. Both elements show thus the behavior of simple solids within the accuracy of all the available results. However, in contrast to the good agreement between shock-wave data and static measurements found for indium[5] and aluminum,[9] marginal

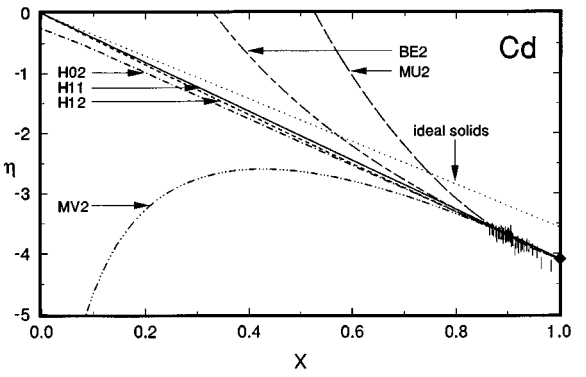

FIG. 16. $\eta-X$ representation of different EOS forms for cadmium. The diamond gives the best value of K_0 derived from ultrasonic measurements (Ref. 44). The bars indicate only the present data.

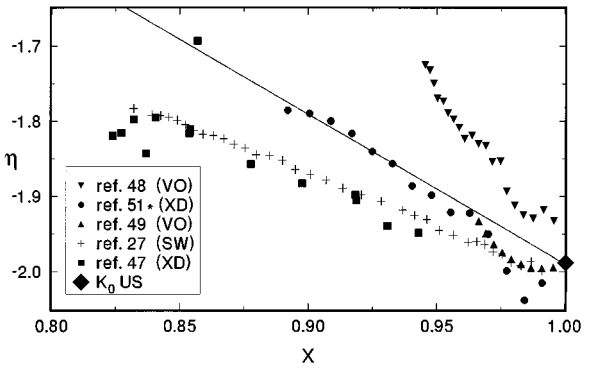

FIG. 17. Comparison of EOS data of magnesium in $\eta-X$ representation. The diamond represents the K_0 value from ultrasonic measurements (Ref. 52). The star denotes rescaled data as discussed in the text.

differences are observed for both these more strongly anisotropic elements, as illustrated by the data in Figs. 11 and 14, as well as by the corresponding parameter values[27] in Table I for Zn in comparison with the ''best'' values derived with H11.

For comparison with the elements zinc and cadmium, literature data for magnesium and beryllium are evaluated in the same way in the next sections. Both these metals show the same $hP2$ structure and strong similarities in their electronic configuration in comparison with Zn, Cd, and Hg (under high pressure). Therefore, these five elements are often considered together as group-II elements.[46]

D. Equation of state of Mg

High-pressure studies on Mg have been performed up to 58 GPa by x-ray diffraction,[47] up to 10 GPa by volumetric measurements[48,49] and up to 55 GPa by shock-wave experiments.[27] At 50 GPa, a phase transition from the $hP2$ structure to the $cI2$ structure was observed[47] and attributed to s-d transfer. The possible volume discontinuity at the transition is smaller than the scatter in the data and can therefore be neglected in the following discussion. Pseudopotential calculations confirmed the transition[50] and also its connection with s-d transfer.

The $\eta-X$ plot of the different data sets for magnesium is given in Fig. 17, which shows large differences between the data. While good agreement is observed between the shock-wave data,[27] the later x-ray data,[47] and some of the volumetric data,[49] significant discrepancies are noticed with respect to the earlier volumetric data[48] and less drastically with respect to the earlier x-ray-diffraction data,[51] which also show some low-pressure anomalies similar to the data of cadmium[20] because of the use of an erroneous value for V_0. Rescaling of the data with a smaller value $V_R=0.022\,75$ nm^3 instead $V_0=0.023\,24$ nm^3 minimizes these deviations. Furthermore, it can be seen from Fig. 17 that the calculated curve using the H11 form and the best value of K_0 from ultrasonic data[52–55] agrees only with these earlier x-ray data,[51] while the shock-wave data,[27] the more recent x-ray data,[47] and some of the volumetric data[49] show much smaller slopes.

These differences can also be seen in the results of fitting the form H12 to these different p-V data sets, as shown in

TABLE III. Parameters for different EOS forms and different EOS data sets of magnesium together with values derived from ultrasonic measurements (US).

K_0 (GPa)	K_0'	p_m (GPa)	σ_V (%)	$-\epsilon$	EOS	Ref.
35(2)	6.3(9)	10	0.08	0.97		48
28(2)	5.9(7)	26	0.42	0.94		51
36(2)	4.6(5)	26	0.18	0.96	H12	51[a]
34(1)	5.0(9)	5	0.04	0.96		49
35.1(7)	3.8(1)	55	0.06	0.96		27
36(2)	3.6(3)	59	1.00	0.89		47
37(2)	3.1(2)		0.58	0.92	MU2	
35(2)	3.8(2)		0.44	0.96	BE2	
35(2)	4.1(3)	55	0.40	0.96	MV2	27, 47, 49
35(2)	3.8(3)		0.44	0.94	H02	
36(2)	3.7(3)		0.47	0.95	H12	
32(2)	4.39(4)		0.75		H11	
32.3						41
35.3						53
35.6					US	55, V
35.5						55, R
34.4						54
35.4	3.9					52

[a]Rescaled data, as discussed in the text.

the upper block of Table III. While reasonable agreement of the values for K_0 is found in all the cases except for the uncorrected earliest x-ray data,[51] only the first set of volumetric data[48] results in a significantly larger value for K_0', whereas the differences for the corrected earliest x-ray data, denoted by the footnote in Table III, and for the later volumetric data[49] with respect to the shock-wave[27] and later x-ray results are marginal. In the plot of the error ellipsoids shown in Fig. 18, only these later data are therefore used. Obviously, these ellipsoids overlap near the best value for K_0 from ultrasonic measurements,[52] and larger deviations of K_0' are related to the larger uncertainties for all the data from limited ranges in pressure.[49,51]

Since there are good reasons to admit that the earliest x-ray-diffraction measurements,[51] as well as the earliest volumetric data,[48] were less accurate than the later measurements, only the later data[27,47,49] were used in the fits of the different EOS forms, which resulted in the data represented in the middle block of Table III. Again, the largest deviations from the best average values for K_0 and K_0' are obtained with the form MU2, which also gives the largest value of σ_V for any of the two-parameter forms. On the other hand, the fit of the one-parameter form H11 results in this case in a much smaller value for K_0 and significantly larger values for K_0' and σ_V.

These differences in the parameters of the form H11 can also be seen in Fig. 18, where the circle for its best-fitting values falls outside the region of overlap of the H12 fits for the different data sets. This observation must be considered as a strong hint that the p-V data of magnesium cannot be

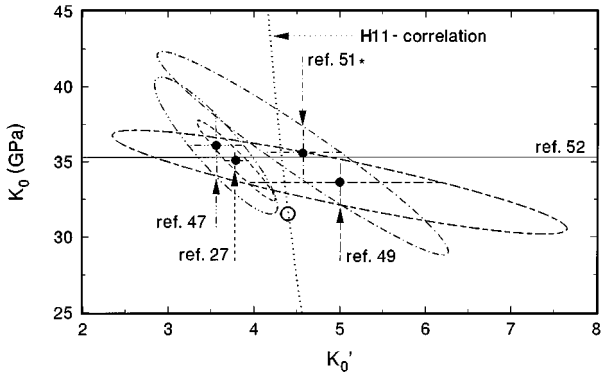

FIG. 18. Error ellipsoids for the parameters obtained by fitting the EOS form H12 to different p-V data sets of magnesium. For details see the text. The star denotes rescaled data as discussed in the text and footnote of Table III.

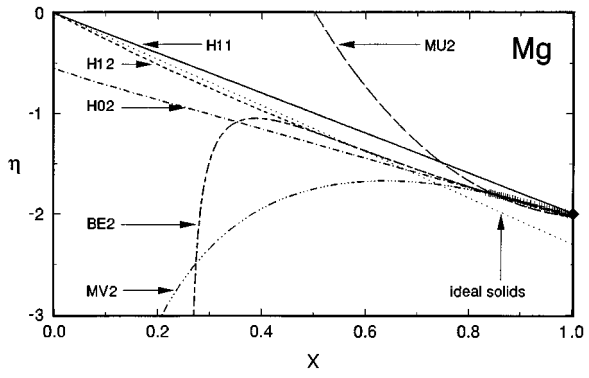

FIG. 19. η–X representation of different EOS forms for magnesium. The diamond gives the best value of K_0 from ultrasonic measurements (Ref. 52). The bars indicate the data of magnesium from shock-wave experiments (Ref. 27).

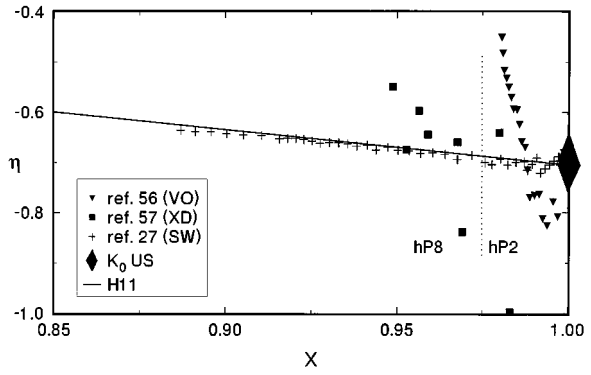

FIG. 20. Comparison of EOS data of beryllium in $\eta-X$ representation. The vertical size of the diamond represents the scatter of the K_0 values from ultrasonic measurements (Refs. 42 and 59–61).

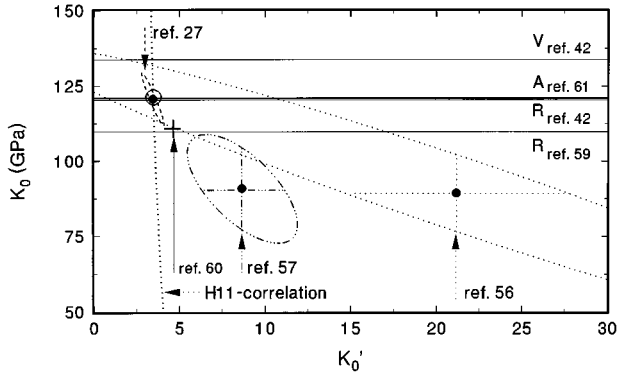

FIG. 21. Error ellipsoids for the parameters obtained by fitting the EOS form H12 to different p-V data sets of beryllium. For details see the text.

described with the one-parameter form H11.

The extrapolations of the different fitted EOS forms in the $\eta-X$ representation of Fig. 19 shows even more clearly the large difference between the first-order form H11 on the one hand and all the other second-order EOS forms on the other hand. Obviously, all these other curves approach the ideal solid behavior rather rapidly; however, the large overshooting of the forms MV2, H02, and finally also BE2 mark the limits for unreasonable extrapolations. The comparison with the ideal solid shows, in the case of magnesium, a positive deviation at low pressures in contrast to the opposite behavior of zinc and cadmium. This means that Mg shows a special hardness at low pressures in comparison with the behavior of an ideal solid.

In summary one can notice that the behavior of Mg under high pressure is very well described by the second-order form H12. The use of the first-order form H11 leads to significant deviations, which may be attributed to the special s-p-type character of this element at lower pressures before some s-d transfer starts to contribute just in the upper range of the available experimental studies.

E. Equation of state of Be

Investigations of the structural behavior of beryllium under strong compression are rather sparse. For EOS data, there are some volumetric measurements[56] up to 10 GPa, x-ray-diffraction measurements[57] up to about 28 GPa, and shock-wave results[27] for the higher-pressure region. The $hP2$ structure at ambient pressure has been reported to transform into a distorted hexagonal structure ($hP8$) at around 11 GPa.[57] From theoretical total-energy calculations, a further transformation to the high-temperature $cI2$ structure is only expected above 100 GPa.[58]

The p-V data for beryllium are represented in the form of an $\eta-X$ plot in Fig. 20, which shows large deviations between the volumetric data[56] and the shock-wave results,[27] especially in the upper range of the volumetric data, while the x-ray data[57] are primarily effected by a large scattering. Close agreement is observed, however, between the ultrasonic data[42,59–61] with their first-order extrapolation with H11 on the one hand and the shock-wave data[27] on the other hand.

Results of unbiased fitting of the form H12 to the data are shown in the upper block of Table IV. K_0' for the volumetric

TABLE IV. Parameters for different EOS forms and different EOS data sets of beryllium together with values derived from ultrasonic measurements (US).

K_0 (GPa)	K_0'	p_m (GPa)	σ_V (%)	$-\epsilon$	EOS	Ref.
89(13)	21(7)	10	0.07	0.99	H12	56
91(8)	9(2)	28	0.56	0.50	H12	57
121(3)	3.4(2)	80	0.04	0.96	H12	27
123(3)	3.1(2)	80	0.07	0.95	MU2	27
120(2)	3.5(1)		0.03	0.94	BE2	
120(2)	3.6(2)		0.03	0.95	MV2	
121(3)	3.4(2)		0.03	0.95	H02	
121(3)	3.4(2)		0.03	0.96	H12	
120(3)	3.47(2)		0.04		H11	
134						42, V
120						42, R
111	4.6				US	60
110						59
121						61

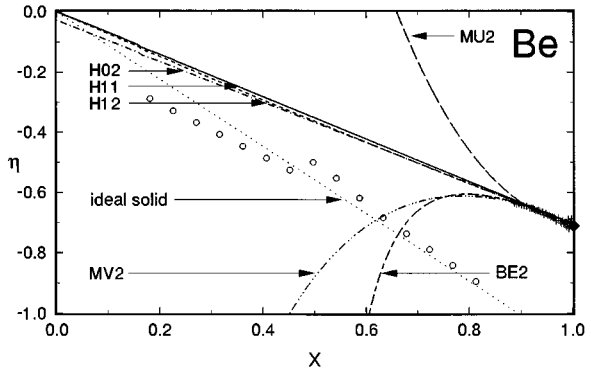

FIG. 22. $\eta-X$ representation of different EOS forms for beryllium. The diamond gives the best value of K_0 from ultrasonic measurements (Ref. 61). The bars indicate the data of beryllium from shock-wave experiments (Ref. 27) and the circles represent theoretical data (Ref. 62).

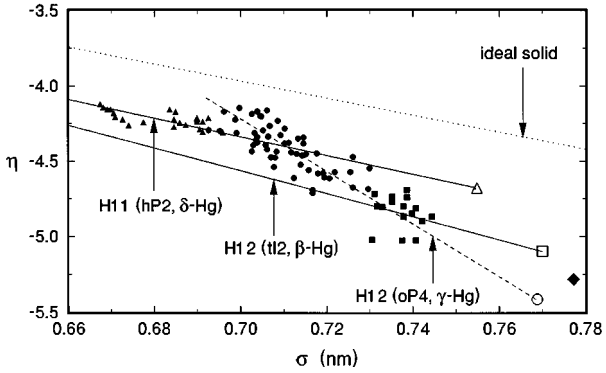

FIG. 23. EOS data of mercury in $\eta-\sigma$ representation. The different symbols refer to the different phases of mercury; the curves represent the corresponding fits to the forms H11 and H12, respectively. Diamond: estimated value of K_0 (Ref. 63).

data[56] is unusually large, but the K_0 value for the shock-wave results[27] compares very well with the best value of K_0 from ultrasonic measurements.[61]

The error ellipsoids in Fig. 21 for these fits show almost no common region of overlap. The shock-wave results show excellent agreement with the best value of K_0 from ultrasonic measurements,[61] represented as horizontal heavier line in Fig. 21. The shock-wave ellipsoid[27] is also intersected by the correlation of the H11 form, which is represented by the dotted line. Because of the large uncertainties of the other data, only the shock-wave results are used in the later discussion.

The fit of the different EOS forms to the data results in the values, which are presented in the second block of Table IV where large deviations of the parameter values for the form MU2 are noticed with respect to the other data. The one parameter form H11 gives the same results as all the other two parameter forms with a value for the bulk modulus very close to the best value derived from the ultrasonic data.

Extrapolations of the different best-fit EOS forms are shown in Fig. 22, again in the form of an $\eta-X$ plot together with theoretical data,[62] which cover an extremely wide range in pressure. While all the forms, H02, H11, and H12, show only minor differences, the forms BE2, MU2, and MV2 diverge rather rapidly into regions of unreasonable values. Compared with an ideal solid, Be shows even larger special hardness than Mg. However, the theoretical data of Be show no special offset and only small variations around the straight line representing the behavior of an ideal solid. The large differences between the theoretical and the experimental data may be attributed to a different value for V_0 used in the theoretical calculations. Furthermore, no x-ray data are available for the region of extremely high pressures to confirm an expected $cI2$ phase. From this point of view, it may be possible that Be in this phase behaves as indicated by the theoretical data, and the p-V data indeed approach the curve of an ideal solid after the predicted phase transition into the $cI2$ structure. In contrast to magnesium, the available high-pressure data of Be are therefore very well described by the first-order form H11 with no advantage of any second-order form.

F. Equation of state of Hg

The behavior of mercury under pressure is dominated by the phase transitions mentioned in Sec. III C of this paper. These phase transitions are all accompanied by special discontinuities of the p-V behavior, as illustrated in Fig. 23, which shows the p-V data of Hg in an $\eta-\sigma$ representation.

Because of the small regions of stability for the low-pressure phases $tI2$ and $oP4$, and because of the rather large scatter of the experimental data for these regions, Fig. 23 shows immediately that it is difficult to determine precise values for the parameters V_0, K_0, and K_0', which are commonly used to fit a given EOS form to the experimental data. The strong correlations between these parameters in the usual fitting procedures thus call for a reduction of the number of free parameters by some reasonable assumption. Therefore, it is tempting to try at first a fit with the first-order form H11, which implies for a high-pressure phase, in addition to the free parameter K_0, also V_0 as free parameter and

TABLE V. EOS Parameter for the different phases of mercury.

V_0 (10^{-3} nm^3)	K_0 (GPa)	K_0'	σ_V (%)	EOS	Phase
24.0(5)	36(5)	6.4(1)	1.80		β-Hg
23.9(5)	45(6)	6.2(1)	2.40	H11	γ-Hg
22.5(5)	61(7)	6.1(1)	0.87		δ-Hg
24.0(5)	35(2)	7.0(1)	1.80		β-Hg
23.9(5)	22(3)	13.5(3)	1.47	H12	γ-Hg
22.5(5)	78(3)	4.2(6)	0.83		δ-Hg

K_0' only as a correlated parameter due to the implicit condition $K_0' = 3 - (2/3)\ln(3K_0/p_{FG0})$ for H11.

The results for the fits of the form H11 to the data for the different phases of mercury are given in the upper block of Table V. From this table one can see that the fitted values for V_0 decrease from one phase to the other, whereas the values for K_0 increase. A relatively small value for σ_V is obtained in this case for the δ-Hg phase; however, the corresponding values for the other two phases are rather large. The next attempt using the second-order form H12 results in the values for V_0, K_0, and K_0' given in the lower block of Table V. The most significant changes are noticed thereby for the orthorhombic γ-Hg phase. The value of the bulk modulus decreases from 45 to 22 GPa, and the anticorrelated pressure derivative K_0' increases to 13.5. The standard deviation σ_V shows a significant decrease by nearly a factor of 2 for this $(oP4)$ γ-Hg phase, but all the values for the $(cI2)$ β-Hg and $(hP2)$ δ-Hg phases are not much affected.

Figure 23 includes as best-fitting curves for the low pressure $(tI2)$ β-Hg phase and high pressure $(hP2)$ δ-Hg phase just straight solid lines corresponding to the form H11, whereas the slightly curved (dashed) line represents the best fit of the form H12 for the intermediate $(oP4)$ γ-Hg phase. For comparison, the behavior of ideal solids is illustrated again by a dotted line, which shows that all the data for mercury fall below this curve, as noted before for cadmium and zinc, however, in contrast to the behavior of magnesium and beryllium, which show much stiffer behavior than the ideal solids.

V. DISCUSSION

The p-V data for these five elements are most reasonable compared with each other in an $\eta - \sigma$ plot, as illustrated in Fig. 24, where the dotted line again represents the behavior of ideal solids, the heavily drawn sections of the continuous curves mark the experimental ranges for each element, and only the data for the $(hP2)$ δ-Hg phase of mercury are included for clarity. In this representation, one can notice that Be, with its pure outer s-p electron configuration, shows a special stiffness (larger values) with respect to the ideal behavior. This special stiffness is already smaller for Mg at ambient pressure, and the special curvature corresponding to the form H12 with a smaller value of K_0' for Mg in comparison with the ideal behavior points to a special change in the electronic structure, which can be attributed to the broadening of the ''empty'' $3d$ band and its partial occupation under increasing pressure. Due to this increase in the mixing of the $3s$, $3p$, and $3d$ electrons in the conduction band of Mg the ideal behavior is obviously approached much more rapidly than either in Be, or in the (heavier) IIb metals, where the fully occupied lower d bands reduce the s-d hybridization in the corresponding conduction bands at least within the present experimental region. The simple EOS behavior corresponding to the H11 form and expressed in Fig. 24 by the straight lines appears thus as another fingerprint for a stable electron configuration, where the unusual c/a ratio of Zn may also be correlated with the special softness of zinc with respect to the ideal behavior, and with correspondingly weaker deviations for Cd and $(hP2)$ δ-Hg.

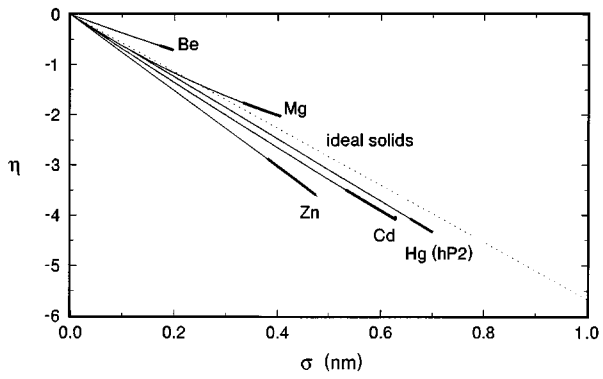

FIG. 24. EOS data represented by the corresponding fitted EOS curves of the group-II elements in $\eta - \sigma$ representation. The length of the thick drawn curves corresponds to the observed compression range.

The structural similarity of the IIb metals, especially under pressure, has already been discussed in earlier publications,[47,64] and it may be sufficient to point out that the structural phase transitions for Be and Mg under pressure are typical for their special band structure as discussed above with respect to their special EOS behavior. The special structural behavior of both Be and Mg under pressure can then be attributed to the lack of core d electrons affecting the conduction band in the IIb cases.

ACKNOWLEDGMENTS

This work was supported by the Bundesministerium für Wissenschaft und Forschung (BMFT) under Contract No. 05 5P PA XB. One of the authors (O. S.) would like to thank the HASYLAB staff for technical help during the stays at HASYLAB.

[1] A. L. Ruoff, H. Xia, and Q. Xia, Rev. Sci. Instrum. **63**, 4342 (1992).
[2] W. B. Holzapfel, in *Molecular Systems under High Pressure*, edited by R. Pucci and G. Piccitto (Elsevier Science, New York, 1991), p. 61.
[3] W. B. Holzapfel, Europhys. Lett. **16**, 67 (1991).
[4] W. A. Grosshans and W. B. Holzapfel, Phys. Rev. B **45**, 5171 (1992).
[5] O. Schulte and W. B. Holzapfel, Phys. Rev. B **48**, 767 (1993).
[6] Y. Vohra and W. B. Holzapfel, High Press. Res. **11**, 223 (1993).
[7] Y. C. Zhao, F. Porsch, and W. B. Holzapfel, Phys. Rev. B **49**, 815 (1994).
[8] Y. C. Zhao, F. Porsch, and W. B. Holzapfel, Phys. Rev. B **50**, 6603 (1994).
[9] R. G. Greene, H. Luo, and A. L. Ruoff, Phys. Rev. B **51**, 597 (1995).
[10] O. Schulte and W. B. Holzapfel, Phys. Rev. B **52**, 12 636 (1995).
[11] W. B. Holzapfel and W. May, Adv. Earth Planetary Sci. **12**, 73 (1982).
[12] W. A. Grosshans, E. F. Düsing, and W. B. Holzapfel, High Temp. High Pressures **16**, 539 (1984).
[13] J. W. Otto (unpublished).
[14] K. Syassen and W. B. Holzapfel, Europhys. Conf. Abstr. **1A**, 75 (1975).

[15] W. B. Holzapfel, in *High Pressure Chemistry*, edited by H. Kelm (Reidel, Boston, 1978), p. 177.
[16] R. A. Forman, G. J. Piermarini, J. D. Barnett, and S. Block, Science **176**, 284 (1972).
[17] H. K. Mao, P. M. Bell, J. W. Shaner, and J. D. Steinberg, J. Appl. Phys. **49**, 3276 (1978).
[18] J. Donohue, *The Structure of the Elements* (Wiley, New York, 1974).
[19] International Union of Pure and Applied Chemistry, *Nomenclature of Inorganic Chemistry, Recommendations 1990* (Blackwell Scientific, Oxford, 1990).
[20] R. W. Lynch and H. G. Drickamer, J. Phys. Chem. Solids **26**, 69 (1965).
[21] O. Schulte, A. Nikolaenko, and W. B. Holzapfel, High Press. Res. **6**, 169 (1991).
[22] S. Meenakshi, V. Vijayakumar, B. K. Godwal, and S. K. Sikka, Phys. Rev. B **46**, 14 359 (1992).
[23] K. Takemura, Phys. Rev. Lett. **75**, 1807 (1995).
[24] W. Potzel, M. Steiner, H. Karzel, W. Schiessl, M. Köfferlein, G. M. Kalvius, and P. Blaha, Phys. Rev. Lett. **74**, 1139 (1995).
[25] P. W. Bridgman, Phys. Rev. **60**, 351 (1941).
[26] S. N. Vaidya and G. C. Kennedy, J. Phys. Chem. Solids **31**, 2329 (1970).
[27] G. C. Kennedy and R. N. Keeler, in *American Institute of Physics Handbook*, 3rd ed. (McGraw-Hill, New York, 1972), pp. 4–38.
[28] O. Schulte and W. B. Holzapfel, Phys. Rev. B. **48**, 14 009 (1993).
[29] O. Schulte and W. B. Holzapfel, Phys. Lett. A **131**, 38 (1988).
[30] F. D. Murnaghan, *Finite Deformation of an Elastic Solid* (Dover, New York, 1967).
[31] F. Birch, Phys. Rev. **71**, 809 (1947).
[32] P. Vinet, J. Ferrante, J. R. Smith, and J. H. Rose, J. Phys. C **19**, L476 (1986).
[33] L. H. Thomas, Proc. Cambridge Philos. Soc. **23**, 542 (1927).
[34] E. Fermi, Rend. Acad. Naz. Lincei **6**, 602 (1927).
[35] W. B. Holzapfel, High Press. Res. **7**, 290 (1991).
[36] G. Queisser and W. B. Holzapfel, Appl. Phys. A **53**, 114 (1991).
[37] W. B. Holzapfel, Physica B **190**, 21 (1994).
[38] W. Voigt, *Lehrbuch der Kristallphysik* (Teubner, Leipzig, 1928).
[39] A. Reuss, Z. Angew. Math. Mech. **9**, 49 (1929).
[40] M. W. Guinan and D. J. Steinberg, J. Phys. Chem. Solids **35**, 1501 (1974).
[41] R. F. S. Hearmon, Rev. Mod. Phys. **18**, 409 (1946).
[42] R. F. S. Hearmon, Adv. Phys. **5**, 323 (1956).
[43] K. S. Alexandrov and T. V. Ryshova, Sov. Phys. Crystallogr. **6**, 228 (1961).
[44] E. Fischer, M. Manghani, and R. Kikuta, J. Chem. Phys. Solids **34**, 687 (1971).
[45] W. P. Mason, *Piezoelectric Crystals and Their Application to Ultrasonics* (Van Nostrand, New York, 1950).
[46] J. Hafner and V. Heine, J. Phys. F **13**, 2479 (1983).
[47] H. Olijnyk, PhD thesis, University Paderborn, 1985.
[48] P. W. Bridgman, Proc. Am. Acad. Arts Sci. **76**, 55 (1948).
[49] S. N. Vaidya and G. C. Kennedy, Phys. Chem. Solids **33**, 1377 (1972).
[50] J. A. Moriarty, Bull. Am. Phys. Soc. **38**, 1551 (1993).
[51] R. L. Clendenen and H. G. Drickamer, Phys. Rev. **135**, 1643 (1965).
[52] E. Naimon, Phys. Rev. B **4**, 4291 (1971).
[53] S. Eros and C. S. Smith, Acta Metal. **9**, 14 (1961).
[54] M. Rosen, Phys. Rev. **174**, 504 (1968).
[55] A. R. Wazzan, and L. B. Robinson, Phys. Rev. **155**, 586 (1967).
[56] P. W. Bridgman, Proc. Am. Acad. Arts Sci. **76**, 71 (1948).
[57] L. C. Ming and M. H. Manghnani, J. Phys. F **14**, L1 (1984).
[58] P. K. Lam, M. Y. Chou, and M. L. Cohen, J. Phys. C **17**, 2065 (1984).
[59] W. D. Rowland and J. S. White, J. Phys. F **2**, 231 (1972).
[60] D. Silversmith and B. Averbach, Phys. Rev. B **1**, 567 (1970).
[61] S. P. Marsh, *LASL Shock Hugoniot Data* (University of California Press, Berkeley, 1980).
[62] J. Meyer-ter-Vehn and W. Zittel, Phys. Rev. B **37**, 8674 (1988).
[63] K. A. Gschneidner, Jr., Solid State Phys. **16**, 275 (1964).
[64] D. A. Young, *Phase Diagrams of the Elements* (University of California Press, Berkeley, 1991).